24Th EUROPEAN ROTORCRAFT FORUM
Marseilles, France - 15th-17th September 1998

REFERENCE : AE 08

TITLE : Experimental and Numerical Investigations of Dynamic Stall at IRPHE/ASI Laboratory

AUTHORS : E. Berton, D. Favier and C. Maresca

IRPHE/ASI Laboratory, UMR 6594 of CNRS, University of Aix-Marseille I & II
163 Avenue de Luminy, case 918, 13009 Marseille, France

This work concerns the experimental and numerical simulation of Dynamic Stall occuring on an airfoil in 2D/3D unsteady flow configuration. The flow unsteadiness is simulated by means of oscillating motions of the airfoil in translation, pitch and combined translation/pitch, which produce variations of velocity V and/or incidence α around the airfoil. The unsteadiness, characterized by overall and local analysis from experiments conducted on a 2D OA209 airfoil and a half-wing of the same airfoil, exhibits the influence of the finite span of the wing. The present results show that the main influence of the finite span is to delay the stalling vortex occurence and to modify the vortex chordwise propagation velocity along the upper surface. This involves a characteristic delay of the dynamic stall incidence and strongly affects the instantaneous behavior of lift, drag and moment. The dynamic stall calculation in the 3D flow configuration has been based on a semi-empirical approach (GBCN code), which consists to apply the 2D version of the GBCN code at the successive spanwise airfoil sections z/h along the half-wing. Comparisons between calculation and experiment concerning the normal coefficient hysteresis loops $Cn=Cn(\alpha)$ are also presented to evaluate the prediction efficiency of this pseudo-3D numerical approach. The present paper also concerns an experimental investigation of the unsteady boundary-layer on a NACA0012 airfoil oscillating in a 2D flow configuration, that aims to bring up some basic data for future Navier-Stokes approach of Dynamic Stall. The study emphasizes on an Embedded Laser Doppler Velocimetry (ELDV) measurement method, suited for unsteady boundary-layer investigation on oscillating airfoils. Using this ELDV method, unsteady features on transition and separation/reattachment of the boundary-layer are investigated in both steady and unsteady flow configurations.

INTRODUCTION

The accurate prediction of unsteady aerodynamics associated with airfoil dynamic stall is of major interest in a wide range of aeronautical applications. For example, the dynamic stall occuring on the retreating blade of an helicopter rotor in forward flight produces significant changes in the airloads and moments spanwise distributions, and thus in the overall rotor performance [1-6]. A proper simulation of the complex blade sections environment requires considering the influence of several parameters, including simultaneous variations in both angle-of-attack $\alpha=\alpha(\omega t)$ and local flow velocity $V=V(\omega t)$, compressibility, blade tip effects, airfoil geometry and sweep angle influence, crossflow and separation phenomena influences, ...

However, due to the complex nature of this 3D unsteady stall phenomenon, previous works in this domain have generally tackled the problem by means of simplified flow configurations, which are simulated to specifically dissociate the different parameters, in order to analyze separately their respective influence. Relevant of such experimental and numerical works are the studies conducted on airfoils oscillating in 2D unsteady flows, and submitted to either pure incidence variations $\alpha=\alpha(\omega t)$ by means of pitching and plunging motions or to pure velocity variations $V=V(\omega t)$ by means of a fore-and-aft translation . To provide a better simulation of the dynamic stall conditions, previous works from the present group [7-10] have concerned the study of dynamic stall generated by means of a combined translation/pitch motion in 2D flows. However, few studies [11-15] have been devoted to investigate the dynamic stall process in 3D flow configurations.

Nowadays, the effort to improve the prediction of drag and moment coefficients in dynamic stall regime has to be focused on Navier-Stokes equations resolution. Modelisation will need more and more experimental flow physics features concerning boundary-layers and criteria on transition and separation. Thus, in order to gain a better

understanding of the boundary-layer response to flow unsteadiness, present works from ASI/IRPHE group are mainly focused on the development of an Embedded Laser Doppler Velocimetry (ELDV) method, suited for unsteady boundary-layer measurements on an oscillating airfoil[16-20]. The measurement principle has been based on an ELDV optical fibres option using an optical head embedded inside the oscillating model, so that the 2D velocity field is directly obtained in the reference frame linked with the moving wall. Such an ELDV method is moreover suited to characterize the unsteady transition, separation and reattachment of the boundary-layer occuring on moving curved walls of oscillating airfoils.

The following sections give a detailed description of the experimental approach and data results, as well as some calculation/experiment comparisons, to exemplify the efficiency of a pseudo-3D numerical approach derived from a semi-empirical 2D code to model the lift hysteresis loops in 3D flow configurations.

EXPERIMENTAL SET-UP AND MEASUREMENT METHODS

As sketched in Figure 1, the experiments are conducted in the S2-Luminy subsonic wind-tunnel of the ASI Laboratory (rectangular test section : 0.5x1 m^2 ; length = 3 m), where the free stream velocity V_∞ can be varied from 2.5 ms^{-1} to 25 ms^{-1} (natural turbulence intensity less than 0.5 %), providing a Reynolds number range based on the model chord from 5.10^4 to 4.10^5.

The generation of independent or simultaneous variations of velocity V and incidence α of the model is realized by means of an original combined translation/pitch motion (Figure 1). The motion in the two degrees-of-freedom is produced by an oscillating device designed to fit beneath the test section floor. The model is supported in a vertical position and attached to the oscillating device by a support shaft located at the quarter chord axis of the model. Different kinds of model motions can be simulated[7] : fore-and-aft translation, plunging, pitching and translation coupled to pitching. Such a device produces variations of relative velocity and incidence as follows :

$V(\omega t) = V_\infty (1 + \lambda \cos\omega t)$

$$\alpha(\omega t) = \alpha_0 + \sum_{n=1}^{5} \Delta\alpha_n \cos(n\omega t + \Phi_n)$$

Moreover the (V,α) cycles are selected from 3D aerodynamics rotor code results, which provide the stalling conditions encountered by the retreating blade sections located at different spanwise stations and for different flight conditions (advancing parameter μ, collective pitch θ, longitudinal and lateral cyclic flap values...). Figure 2 gives the simulation domain of parameters ($\lambda = A\omega/V_\infty$, $k = c\omega/2V_\infty$) that can be covered by the capabilities of the present experimental facilities. The (λ,k) cases numbered from 1 to 6, have been more specifically investigated in the present study.

In a first experimental approach, the simulation is conducted on a OA209 oscillating airfoil with values of λ and k parameters located at the lower and upper limits of the flight domain.

In the 2D flow configuration, the tested airfoil consists in a rectangular wing of 0A209 profile (chord c = 0.2m; span h = 0.495 m) spanning the entire test section. In the 3D flow configuration the model consists in an half-wing of same 0A209 profile and chord (c = 0.2 m), with h = 0.40 m for span (see Figure 3). The same oscillating motions are given to either the complete wing (2D) or the half-wing (3D) and the results already obtained in the 2D case [8-12] are used as a reference basis to investigate both the finite span effect and the influence of unsteadiness on the half-wing behavior.

On both models (2D or 3D), overall measurements of instantaneous lift, drag and moment coefficients are carried out by means of a 3-components balance statically and dynamically calibrated, embedded with the oscillating device. Local measurements of pressure distributions along upper side and lower side of the model, are measured by means of miniature unsteady pressure transducers mounted flush with the airfoil surface. In the 2D flow case, the model is instrumented along the chordwise section with 18 transducers located at mid span of the wing. The 3D half-wing was built by stacking different elements as sketched in Figure 3. One of these elements was equipped with 18 pressure transducers. Local chordwise distributions can thus be measured at different section along the half-wing span by moving the instrumented section. Four spanwise sections were considered : numbered 1, 2, 3, 4 in Figure 3 and located at z/h = 0.50 ; 0.62 ; 0.74 and 0.86 along the span. More details concerning the measurement techniques and the data reduction procedures can be found in references 8-12.

The second experimental approach concerns more specifically unsteady boundary-layer measurements on a NACA0012 airfoil model which oscillates according to the following motions :

- Pitching motion (instantaneous incidence variation around a mean incidence) : $\alpha(t) = \alpha_0 + \Delta\alpha\cos\omega t$,
- Translation motion (instantaneous velocity variation) : $U_{rel}(t) = U_\infty + A\omega\cos\omega t$,
- Combined translation/pitch motion: $\alpha(t) = \alpha_0 + \Delta\alpha(\cos\omega t + \phi)$, $U_{rel}(t) = U_\infty + A\omega\cos\omega t$.

Steady and unsteady measurements of the (u,v) velocity profiles have been performed at different distances from the leading edge along the upper-side of the airfoil, for 3 chordwise locations (s/C=0.3, 0.508, 0.67). The upstream Reynolds number is fixed at $Re=10^5$.

The NACA0012 airfoil is 30 cm in chord, 49.5 cm in span and 3.6 cm in thickness (see Figure 4). The optical head is mounted on a supporting turntable which is attached to the oscillating frame as shown in Figure 4. The optical head is equipped with a beam-expander to increase the focal distance up to 400 mm, so that the laser beams are focusing at mid-span in the boundary-layer through a 45° mirror. Due to the fact that the supporting turntable is linked with the oscillating frame, the u and v velocity components are directly measured in the reference frame in relative motion.

Moreover, the optical head is also installed on an automatized 2D-displacement device mounted itself on the circular turntable. This teledriven system allows the adequate positioning of the measurement volume at any point of the airfoil surface (30 cm in chordwise displacement). An angular sector (from 0° to 360° by step of 0.1°) provides [18-20] the selection of the surveying normal direction, and the laser measurement volume can then be displaced along the local normal to the surface from y = 0.2 mm to y = 145 mm with a displacement accuracy of 0.1 mm.

Figure 5 presents the acquisition chain of the bidimensional ELV system operating in the back scatter mode. Data acquisition is made on a micro-computer from two Burst Spectrum Analysers delivering for each velocity component (u, v) the Doppler frequencies and the arrival validation time for each frequency measurement. The software (COMBSA) used for acquisition and data reduction has been developed at ASI Laboratory [18-20] under Apple-LabVIEW system. The unsteady data reduction technique is made using an ensemble average procedure suited for periodic flows investigation.

Due to the periodicity of the flow, each period is considered as a specific sample of the same phenomenon, so that each velocity component, u(t) or v(t), can be obtained at each phase angle ωt as the averaged value of the velocity samples recorded at the same given phase angle and over a large number (higher than 150) of cycles of oscillation. The simultaneousness of the 2D measurement is then obtained from a synchronisation procedure of the acquisition chain, providing the phase averaged value of the mean velocity components and their associated turbulent quantities [18-20]. Concerning the seeding of the flow, rates of data validation of about 500 Hz are obtained using a mixture of alcohol and glycerine producing particles of about 2 μm in diameter. The freestream flow is seeded by means of a streamlined tube located in the suction chamber of the wind-tunnel (see Figure 1).

NUMERICAL APPROACH

When the model oscillates in the 2D flow configuration, the dynamic stall calculation method of semi-empirical nature is derived from the phenomenological model initially developped in Ref. 21 for an airfoil oscillating in pitch through stall. To take into account the simultaneous (V, α) variations generated by the combined translation/pitch motion of the model, the differential equations system has been expressed in terms of circulation and derivatives on time [9-12]. The calculation code obtained (so-called GBCN) also accounts for the quasi-steady lift behavior of the 0A209 airfoil in steady flows conditions. Additionally, the derivation of a mathematical optimisation method for determining the set of constants to be introduced in the differential equations system has been also included in the GBCN code [11-12]. The present GBCN code is shown to provide an excellent description of the instantaneous lift hysteresis loops generated by the translation/pitch motion for stalling conditions in 2D flows.

When the model oscillates in combined translation/pitch motion in the 3D flow case, the present numerical approach consists to apply the 2D GBCN calculation model at the successive spanwise sections z/h = constant of the half-wing. All the quasi-steady lift behaviors of the 4 sections into consideration are then deduced from the experimental data base, and the optimization procedure for determining the set of constants is applied at each section z/h along the half-wing span.

RESULTS AND DISCUSSION

OA209 AIRFOIL IN TRANSLATION/PITCH COMBINED MOTION

To exemplify the experimental results obtained on the airfoil oscillating in the 3D flow case, the following data will concern the cycle variations (V,α) shown in Figure 2. For instance, Figure 6 gives the (V,α) variations of case 1, for a mean value α_0 = 14.16° and quite low values of λ and k. Consequently the unsteady effects generated on the model at such values of the oscillating parameters remain moderate but are shown to be much accentuated when increasing the values of $\Delta\alpha n$, λ and k.

The model response to the (V, α) variations of case 1 for 4 different values of the mean incidence α_0 = 6° ; 9° ; 12° ; 14.16°, is given in Figure 7. The plots represent the evolution as a function of ωt of the instantaneous overall coefficients (C_l, C_d, C_m) obtained in the 2D/3D flow configuration. At each given incidence α_0 = constant, the results indicate that the dynamic stall incidence value α_{DD} is higher in the 3D flow case than in the 2D flow case. Additionally the phase ωt of stall occurence in the 3D flow case, is delayed when compared to the 2D flow case. For instance at α_0 = 9°, the stalling incidence is α_{DD}= 14° and occurs at ωt = 45° in 2D flow, while in the 3D flow (Figure 7), α_{DD} = 15° and occurs at ωt = 60°.

Moreover when compared to the 2D case, the results obtained on 3D stall also exhibit a strong attenuation of the amplitudes variations of the C_l coefficient. On the other hand the C_d amplitudes variations are quite similar in both configurations. The nose-down effect on the Cm coefficient is also less intense in the 3D case.

The boundary-layer reattachment which corresponds to the occurence of positive value of Cm coefficient (nose-up) is shown to be generated at a phase $\omega t \approx 225°$ quite similar in both flow configurations. Consequently the half-wing is shown to stall along a part of the period which is shortened compared to the 2D case. Figure 8 illustrates the aerodynamic airloads variations with the instantaneous incidence α, obtained in 2D and 3D flow configurations. As previously mentioned, the 3D effects are shown to significantly increase when the oscillating parameter values (λ, k, $\Delta\alpha n$) increase (case 5 in Figure 8).

Concerning the stalling vortex propagation along the upper surface of the OA209 model for case 1, a comparison of results obtained in the 2D/3D flow configurations is shown in Figure 9. In this Figure the pressure waveforms $Cp=Cp(\omega t)$ are plotted either in the 2D flow case or at 3 different sections z/h = 0.62 ; 0.74 ; 0.86 in the 3D flow case. The phenomenology of the stall process is quite similar in both configurations (e.g. the occurrence and propagation of a strong upper side vortex along the chord of the model). Moreover the plots in Figure 9 reveal the imprints of the vortex by the successive pressure peaks on the Cp-waveforms. The vortex emission generated in the 3D case is thus shown to be shifted between phases ωt = 15° and ωt = 33° when the spanwise position increases towards the half-wing tip.

Figure 10 illustrates the unsteady mean Cp-distributions (averaged over a period) obtained in the 3D flow case as a function of the spanwise position z/h of the airfoil section. The 3D effects are shown to be more accentued when z/h increases and to produce a decrease of the unsteady mean Cp-distributions both on the upper side and the lower side of the airfoil section, confirming the loss of unsteady mean lift as deduced from the overall measurements in Figure 8.

Figure 11 gives an example of comparisons between calculation and experiment concerning the normal force coefficient Cn at different sections of the span varying from z/h = 0.50 to z/h = 0.86. The Cn hysteresis loops calculated by the GBCN code previously discussed, are shown to be in good agreement with the experimental Cn (deduced by integration of instantaneous Cp-distributions measured at each z/h = constant). The main divergence between calculation and experiment is shown to occur in the wing tip region (z/h = 0.86) where the tip vortex path has a strong influence on the local loading distribution. For this wing span region, the results clearly show the limitations of the present pseudo-3D approach and indicate that the combined influences of the wing finite span, the tip vortex formation, and the flow unsteadiness have to be taken into account for an adequate modelling of the Cn-hysteresis loop behavior near the wing tip.

UNSTEADY BOUNDARY-LAYER CRITERIA

This section of the paper, focused on an experimental investigation of the unsteady boundary-layer on a NACA0012 airfoil oscillating in a 2D flow configuration, aims to point out useful data for future Navier-Stokes dynamic stall calculations. Unsteady flow features on transition and

separation/reattachment of the boundary-layer are investigated in both steady and unsteady flow configurations.

Steady flow configuration

Considering first the steady NACA0012 airfoil, Figure 12 presents the evolution of the boundary-layer velocity components (u,v) measured as a function of y (normal distance to the model wall) at the reduced abscissa along the chord s/c=0.67 and for different values of the mean incidence α_0, $0°\leq\alpha_0\leq18°$. The upstream Reynolds number is fixed at $Re=10^5$ and corresponds to a freestream velocity U_∞=5 m/s. Figure 12 shows an attached boundary-layer behavior for $0°\leq\alpha_0\leq12°$, where the tangential and normal velocities (u,v) remain both positive. From α_0=15° to 18°, the velocity profiles reveal a separation of the boundary-layer (negative values of (u,v)) which strongly increases the values of the boundary-layer thickness δ.

The development of the steady boundary-layer along the upper-surface of the airfoil is also presented in the Figure 13 for a fixed incidence $\alpha_0=12°$ at $Re=10^5$. For 3 values of s/c (s/c=0.3 ; 0.508 ; 0.67), Figure 13 presents the evolution of the (u,v) velocity profiles as a function of y and shows that for a fixed value of y, the tangential and normal velocities (u,v) increase as s/c decreases.

Unsteady flow configuration

The translation motion effect on the boundary-layer evolution is illustrated through the oscillating conditions which involves instantaneous velocity variation with $\alpha_0=6°$, $Re=10^5$, $\lambda=0.251$, $k=0.188$. The evolutions of u=u(y) and v=v(y) along the period, are plotted in Figure 14 for 8 phase values ωt ($0°\leq\omega t\leq360°$), and 3 s/c (s/c=0.3 ; 0.508 ; 0.67).

As for the steady flow case, Figure 14 shows that the mean local external velocity U_e is more important at the reduced abscissa located near the leading edge of the airfoil (s/c=0.3) when compared with the U_e value relative to s/c=0.508 and 0.67. It can also be noted that all along the period, the decrease in U_e is linked with the increase of the boundary-layer thickness δ. This phenomenon is due to the decrease of the pressure gradient associated to the local airfoil curvature along the chord. Moreover, considering the entire oscillation cycle, it appears clearly that the velocity components (u, v) reach their minimal values at nearly the same phase of oscillation (ωt=180°).

For the same conditions of the fore-and-aft motion, Figure 15 presents the evolution of the $u/Ue=u/Ue(\eta)$ profiles along the oscillation period at $\alpha_0=6°$ and s/C=0.67. The velocity measurements obtained in this case, are well matched by theoretical velocity profiles corresponding to transitional or turbulent boundary-layer (1/N laws).

The characteristic evolution of the $u=u(y,\omega t)$ velocity profile during a cyclic separation/reattachment process, is clearly exhibited in Figure 16 for the following parametric conditions of the pitching motion : $\alpha_0=12°$, $\Delta\alpha=6°$, $Re=10^5$, $k=0.188$. At the 3 s/c into consideration, the phases ωt corresponding to an attached boundary-layer regime, range over more than the half of the period ($135°\leq\omega t<360°$).

As shown by the plot corresponding to ωt=315° and ωt=0° (Figure 16), the separation process is initiated prior to the maximum incidence value ($\alpha_0=18°$) and is shown to propagate from the leading edge of the NACA0012 airfoil. At ωt=0°, the intensity of the separated flow velocity region is more important at s/c=0.3 and 0.508 when compared to the reduced abscissa s/c=0.67.

During the incidence downstroke of the pitching motion (see also Figure 16), the separation of the boundary-layer concerns the whole upper-side region of the airfoil (ωt=45°, ωt=90°). The dynamic reattachment of the boundary-layer is then initiated from the leading edge and propagates all along the upper-side of the airfoil (ωt=135°).

The Sandborn & Kline separation criterion [22], previously checked to characterize the separation process occurring on the NACA0012 airfoil either in steady flow or in pitching motion [7-9], has been also applied in Figure 17 to the present pitching oscillation conditions. This criterion, based on the instantaneous shape factor H which is expressed as a function of $\delta1/\delta$, is able to differentiate intermittent from fully developed separation regimes.

From the results of Figure 17, it is shown that the Sandborn & Kline criterion appears to be well suited to delimit the attached boundary-layer regime (black symbols) and the separated flow regimes (white symbols) in the case of pitching motion. However, within the separated zone, the criterion appears to be less efficient in differentiating the intermittent

separation from the attached boundary-layer regime. The plots in Figure 17 indeed show that the phase $\omega t=135°$, which corresponds to an attached boundary-layer, is identified by the criterion as an intermittent separation.

Concerning the influence of the superposition of incidence and velocity variations, the unsteady boundary-layer behavior is analyzed on Figures 18 and 19. Figure 18 presents the evolutions of u=u(y) for 8 successive phases ωt along the oscillation period, at the 3 reduced abscissa s/c=0.3, 0.508, 0.67. The parametric conditions of the combined motion correspond to a velocity/incidence coupling in phase ($\phi=0°$) at $\alpha_0=6°$, $\Delta\alpha=6°$, $Re=10^5$, $\lambda=0.251$, $k=0.188$.

As for the pitching case, the plots corresponding to $\omega t=315°$, 0°, 45°, show an increase of the boundary-layer thickness δ when s/c is increasing on the upperside of the airfoil towards the trailing edge direction. It can also be noted, that this growth of δ is linked with the decrease of the mean local external velocity U_e.

The validation of the unsteady transition criterion established in previous [16-18] works on flat plate model and on a NACA0012 airfoil oscillating in pitching motion, has been extended here to the translation/pitch combined motion. This criterion is based on the integral energy thickness parameter δ'_3, and is formulated as shown in Figure 19.

An example of such an extension which confirms the validity of the above criterion for the conditions of unsteadiness generated by the combined motion is shown in Figure 19, corresponding to the oscillating conditions previously mentioned. The boundary-layer survey is performed in this case at s/c = 0.67.

In Figure 19, the instantaneous values of $R\delta'_3$ are plotted as a function of Re_s at different phases of the period. The $R\delta'_3$ evolution is shown to be like an hysteresis loop in the Re_s-$Re\delta'_3$ diagram which is typical of the instantaneous transitional response of the boundary-layer as a function of the unsteadiness parameters (k,λ) generated by the forced airfoil motion. The results clearly indicate the capability of the transition criterion in delimiting accurately the laminar regime (white symbols) from the transitional/turbulent regime (black symbols), as a function of phase ωt.

CONCLUSIONS

The present paper has presented an experimental and numerical investigation of the airfoil dynamic stall in a 2D/3D unsteady flow configuration. The aerodynamic response of a half-wing (OA209 airfoil) submitted to stall generated by simultaneous variations of velocity V and incidence α, has been characterized from local and overall instantaneous measurements. From the overall measurements performed on the half-wing, an increase in the dynamic stall incidence value α_{DD} is obtained when compared to the 2D stalling conditions. The local pressure measurements $Cp=Cp(\omega t,x/c,z/h)$ have shown that the stalling vortex occurence is delayed along the period when the spanwise sectional position z/h increases towards the wing tip.

A numerical approach of the normal coefficient loops $Cn=Cn(\alpha)$ generated through stall in the 3D flow, has been derived in the present study using the GBCN model at different spanwise sections z/h of the half-wing. A good agreement between the GBCN code results and the measured Cn-loops has been obtained all along the wing span excepted for the regions very close to the tip. An improvement in modelling the combined influences of the tip vortex formation and development, the finite span of the wing, and the flow unsteadiness are required for this region of the span.

In a second part, the Embedded Laser Doppler Velocimetry (ELDV) method has been successfully applied to 2D velocity measurements (u, v) both in steady flow case and around a moving airfoil oscillating in pitch, translation, and translation/pitch combined motions. Using this ELDV method, the boundary-layer dynamic behavior and the specific local unsteady flow features relative to separation and transition, have been investigated over a large range of non-steady parametric conditions. The experimental results, so obtained, will constitute an useful data base for future Navier-Stokes dynamic stall calculations.

NOMENCLATURE

A	oscillation amplitude of the model, (m).
c, C	chord of the model, (m).
Cd	drag coefficient, ($Cd=T/0,5\rho SV^2$).
Cl	lift coefficient, ($Cl=T/0,5\rho SV^2$).
Cm	pitch moment coefficient,($Cm=M/0,5\rho SV^2$).
Cn	normal force coefficient, ($Cn=Fn/0,5\rho SV^2$).
Cp	pressure coefficient, ($Cp=p-p\infty/0,5\rho V^2$).
f	frequency of oscillation, (Hz).
H	integral shape factor ($H=\delta_1/\delta_2$).
k	reduced frequency of oscillation, ($c\omega/2U_\infty$).

k	reduced frequency of oscillation, $(c\omega/2U_\infty)$.
Re	Reynolds number, $(U_\infty c/\nu)$.
Re_s	local Reynolds number, $(U_e(s,t)s/\nu)$.
s	curvilinear distance along the wall from the airfoil leading edge, (m).
t	time, (sec).
u	instantaneous tangent velocity (parallel to the wall), (ms^{-1}).
U	mean velocity tangent to the wall, (ms^{-1}).
U_e	mean local external velocity, (ms^{-1}).
U_∞	freestream velocity, (ms^{-1}).
$U_{rel}(t)$	flow velocity due to the fore-and-aft motion, (ms^{-1}).
v	instantaneous velocity normal to the wall, (ms^{-1}).
V	mean velocity normal to the wall, (ms^{-1}).
y	normal distance to the model wall, (m).
α	instantaneous incidence of the model, (deg).
α_0	mean incidence of the model, (deg).
α_{DD}	dynamic stall incidence of the model, (deg).
α_{DS}	static stall incidence of the model, (deg).
δ	boundary-layer thickness, (m).
δ_1	integral displacement thickness, (m).
δ_2	integral momentum thickness, (m).
δ_3	first integral energy thickness, (m).
δ'_3	second integral energy thickness, (m).
$\Delta\alpha$	angular amplitude relative to the pitching motion, (deg).
ϕ	phase shift between velocity and incidence oscillations, (deg).
η	reduced Blasius normal distance, $(y\sqrt{Re_s}/s)$
λ	reduced amplitude relative to the fore-and-aft motion, $(A\omega/U_\infty)$.
ν	kinematic viscosity, (m^2s^{-1}).
ω	angular frequency, $(2\pi f)$, $(rads^{-1})$.
ωt	phase of the period, (deg).

ACKNOWLEGMENTS

The authors wish to thank the support provided by the "Direction des Recherches Etudes et Techniques" under Grant 95/052.

REFERENCES

1-MARESCA, C., FAVIER, D., REBONT, J., "Experiments of an Aerofoil at High Angle of Incidence in Longitudinal Oscillations", Journal of Fluid Mechanics, Vol. 92, Part 4, 1979.

2-Mc CROSKEY, W.J., "The Phenomenom of Dynamic Stall", NASA TM 81264, March 1981.

3-ERICSON, L.E., REDING, J.P., "Unsteady Flow Concepts for Dynamic Stall Analysis", Journal of Aircraft, Vol. 21, N° 8, pp. 601-606, August 1984.

4-REDDY, T.S., KAZA, K.R., "A Comparative Study of Some Dynamic Stall Models", NASA TM 88917, March 1987.

5-FAVIER, D., AGNES, A., BARBI, C. and MARESCA, C., "Combined translation/pitch motion : a new airfoil dynamic stall simulation.", Journal of Aircraft, Vol. 25, N° 9, pp. 805-814, 1988.

6-LEISHMAN, J.G., BEDDOES, T.S., "A Semi-Empirical Model for Dynamic Stall", Journal of American Helicopter Society, Vol. 34, pp. 3-17, July 1989.

7-FAVIER, D., MARESCA, C., REBONT, J., "Dynamic Stall due to Fluctuations of Velocity and Incidence", A.I.A.A. Journal, Vol. 20, n° 7, pp. 865-871, July 1982.

8-FAVIER, D., AGNES, A., BARBI, C., MARESCA, C., "The Combined Translation Pitch Motion : A New Airfoil Dynamic Stall Simulation", Journal of Aircraft, Vol. 25, n° 29, pp. 805-814, September 1988.

9-FAVIER, D., BELLEUDY, J., MARESCA, C., "Influence of Coupling Velocity and Incidence Variations on the Airfoil Dynamic Stall", Proceedings of AHS 48th Annual Forum, pp. 1385-1407, June 1992.

10-PETIT, L., PASCAZIO, M., VINGUT, G., FAVIER, D., "Simulation Experimentale et Numérique sur Profil Oscillant en 2D du Décrochage Dynamique d'une Pale de Rotor d'Hélicoptère", La Recherche Aérospatiale, Vol 1, pp. 29-46, Janvier 1995.

11-FAVIER, D., MARESCA, C., PAGANOTTO, C., VINGUT, G., "Simulation du Décrochage Dynamique de Profils en Ecoulement Instationnaire 2D/3D", STPA Contract 93/91023, Final report, June 1995.

12-PAGANOTTO, C., FAVIER, D., MARESCA, C., BERTON, E, AGNES, A., "Airfoil dynamic stall investigation in 3D unsteady flow", A.I.A.A., Proceedings of the 14th Applied Aerodynamics

Conference, A.I.A.A. paper n° 96/2513, Part. 2, pp. 1098-1105, New Orleans, June 1996.

13-PIZIALI, P.A., "2D and 3D Oscillating Wing Aerodynamics for a Range of Angles of Attack Including Stall", NASA TM 4632, September 1994.

14-COSTES, J.J., "Aerodynamic Moments on Rotor Blades in Forward Flight Test Results and Modeling", Proceedings of the 21st European Rotorcraft Forum, Paper n°2-2, Saint Petersburg, September 1995.

15-GALBRAITH, R.A., COTON, F.N., JIANG, D., GILMON, R., "Preliminary Results From 3D dynamic Stall experiments of a Finite Wing", Proceedings of the 21st European Rotorcraft Forum, Paper n° 2-3, Saint Petersbourg, September 1995.

16-FAVIER, D., MARESCA, C. and BELLEUDY, J., "Unsteady flows around an oscillating flat plate model using an embodied technique of fibre optics laser velocimeter.", Proceedings of the 17th Congress of Aeronautical Sciences, I.C.A.S.-A.I.A.A., Stockholm, September 1990.

17-FAVIER, D., MARESCA, C., RENON, P. and AUTRIC, J.M., "Boundary-layer measurements on oscillating models using an optical fibre LDA technique", Proceedings of the 6th International Symposium on Applications of Laser Techniques to Fluid Mechanics, Lisbon, July 1992.

18-PASCAZIO, M., STEINHOFF, J., BERTON, E., FAVIER, D., "Influence of coupling incidence and velocity variations on the airfoil dynamic stall, comparisons between Navier-Stokes calculations and experiments", A.I.A.A., Proceedings of the 33rd Aerospace Sciences Meeting, AIAA Paper N° 95-0310, Reno, January 1995.

19-FAVIER, D., MARESCA, C. and BERTON, E., 1996, "Etude expérimentale et numérique du développement de la couche limite instationnaire sur modèles oscillants en écoulement 2D/3D.", D.R.E.T. Contract n° 95/052, Synthesis Report.

20-BERTON, E., FAVIER, D., MARESCA, C., "Embedded L.V. methodology for boundary-layer measurements on oscillating models", A.I.A.A., Proceedings of the 28th Fluid Dynamics Conf., A.I.A.A. paper n° 97/1832, Snowmass, June 1997.

21-PETOT, D., "Modelisation du décrochage dynamique par équations différentielles", La Recherche Aérospatiale, Vol. n° 5, Juin 1989.

22-SANBORN, V.A. and KLINE, S.J., "Flow Models in Boundary-Layer Stall Conception", J. Basic Eng., pp. 317-327, 1961.

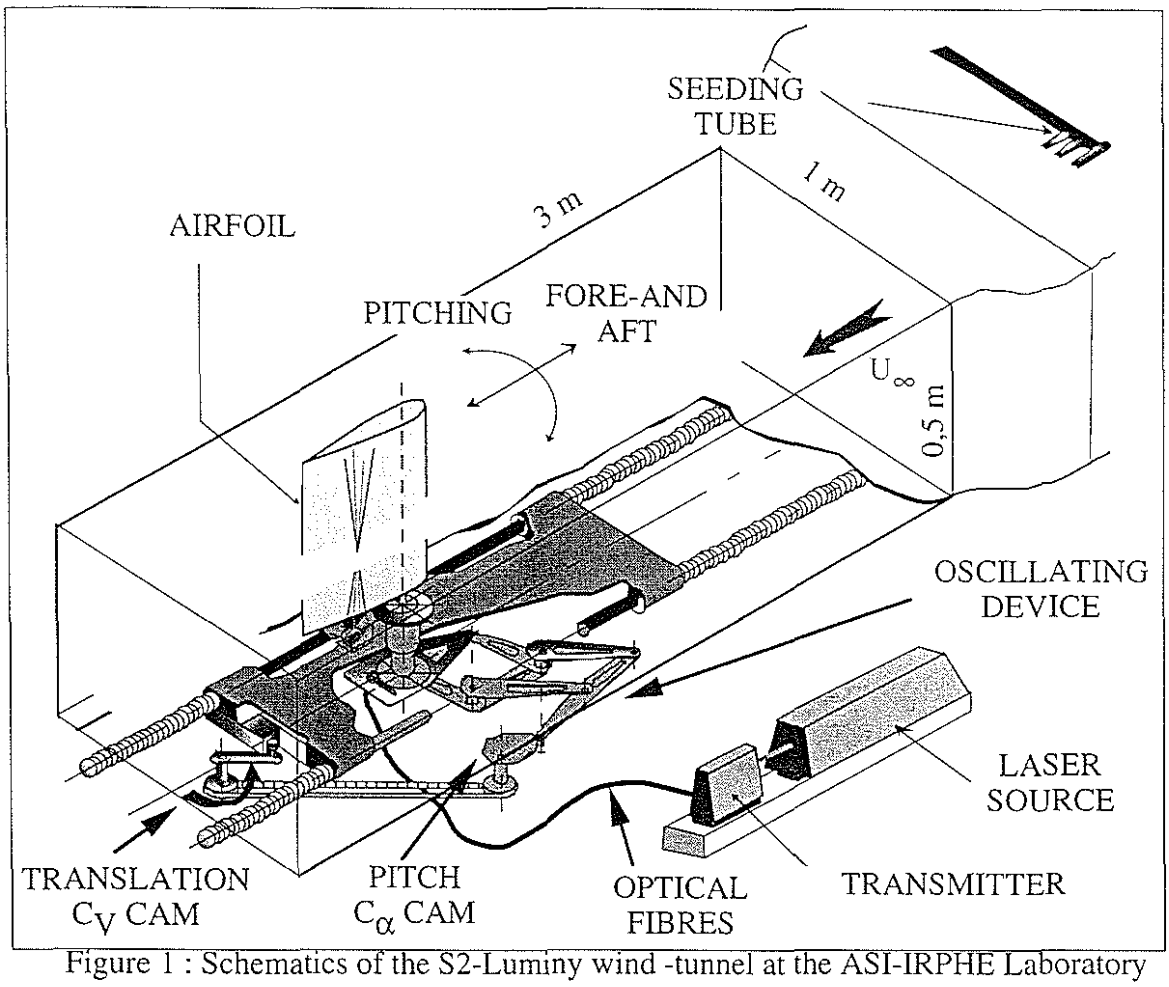

Figure 1 : Schematics of the S2-Luminy wind -tunnel at the ASI-IRPHE Laboratory

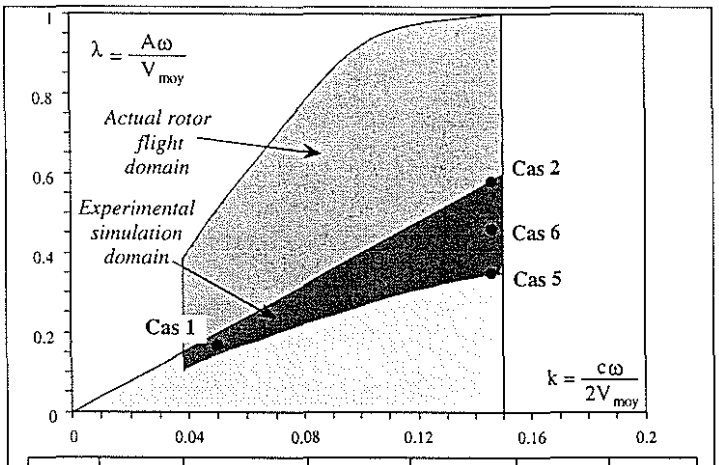

CASE	A(m)	Vmoy(m/s)	f(Hz)	αo(nom)	λ	k
1	0,34	12,56	1,0	14,16°	0,170	0,050
2	0,40	5,20	1,2	15,50°	0,580	0,146
5	0,24	5,20	1,2	10,20°	0,350	0,146
6	0,32	5,16	1,2	11,94°	0,465	0,146

Figure 2 : Simulation of dynamic stall conditions within the rotor flight domain.

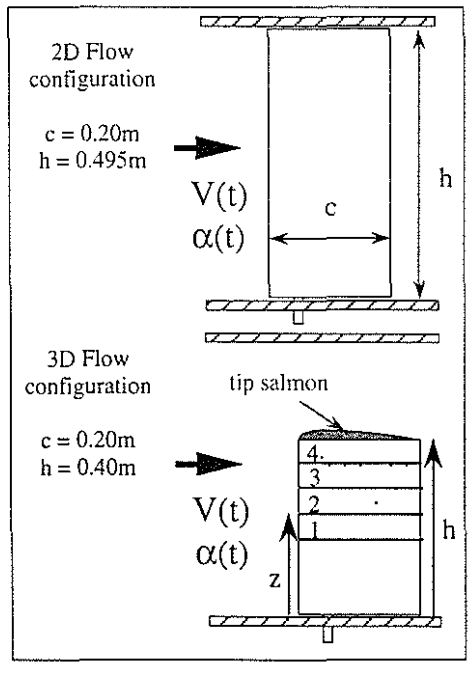

Figure 3 : Schematics of 2D and 3D wings

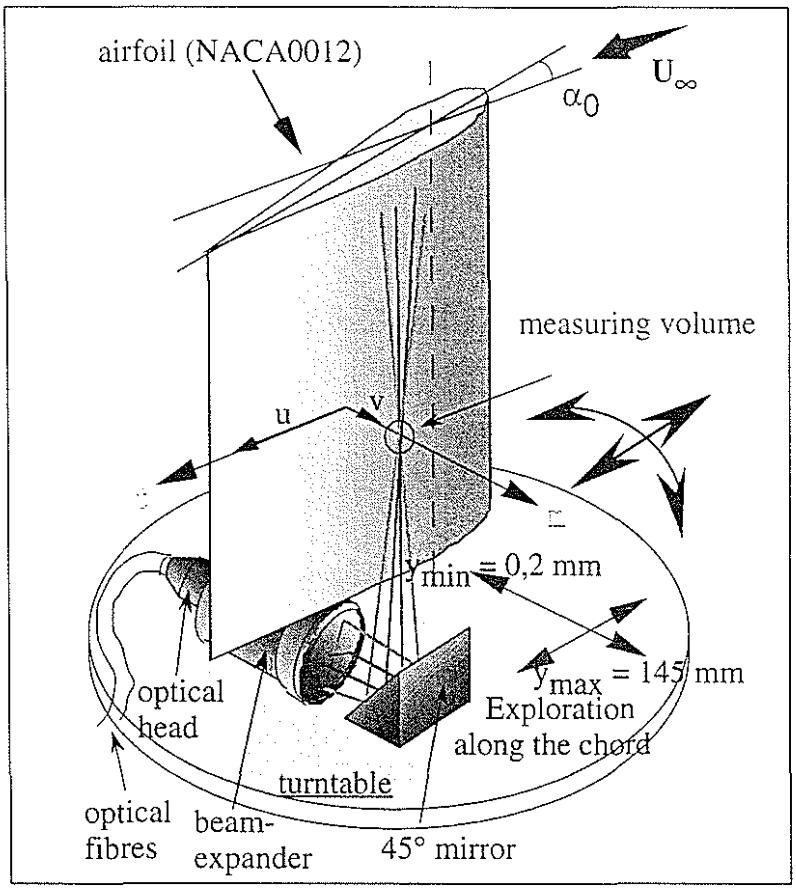

Figure 4 : NACA0012 airfoil - Embedded measurements linked with the oscillating frame model.

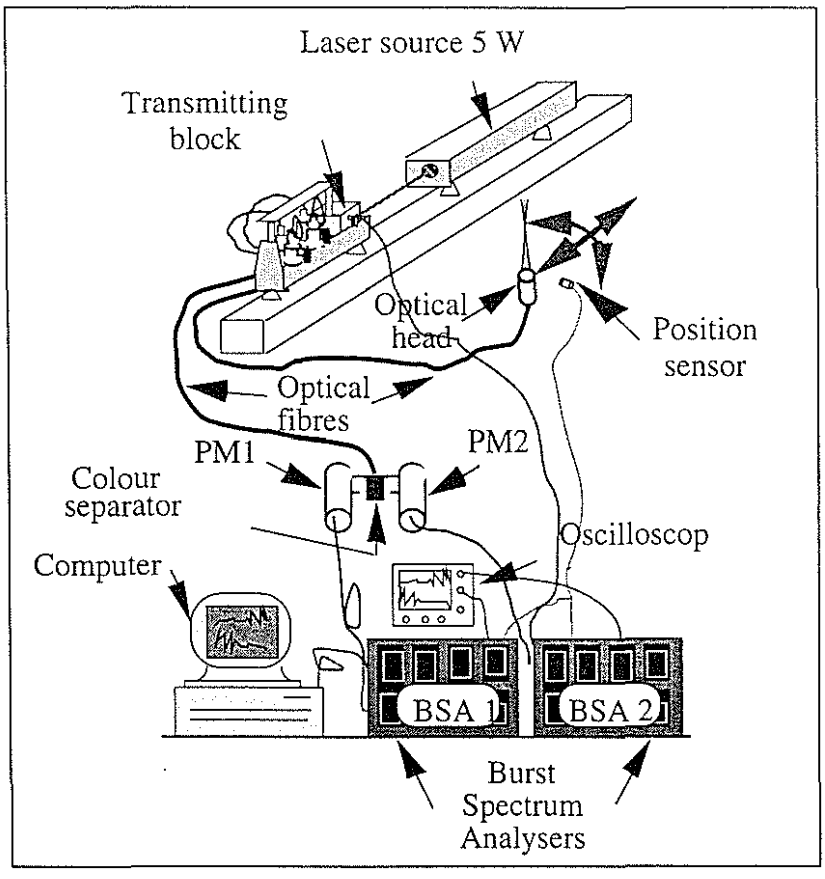

Figure 5 : ELDV data acquisition chain.

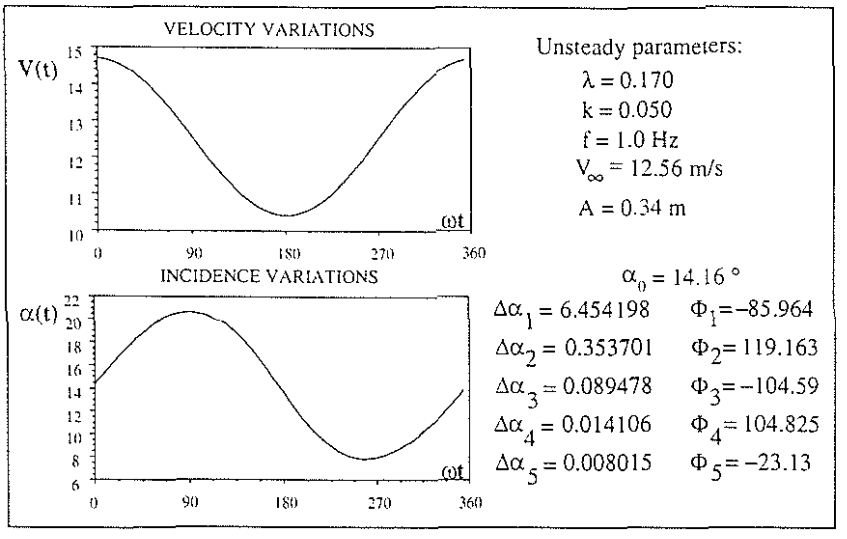

Figure 6 : Parametric conditions of variations (V,α) for case 1.

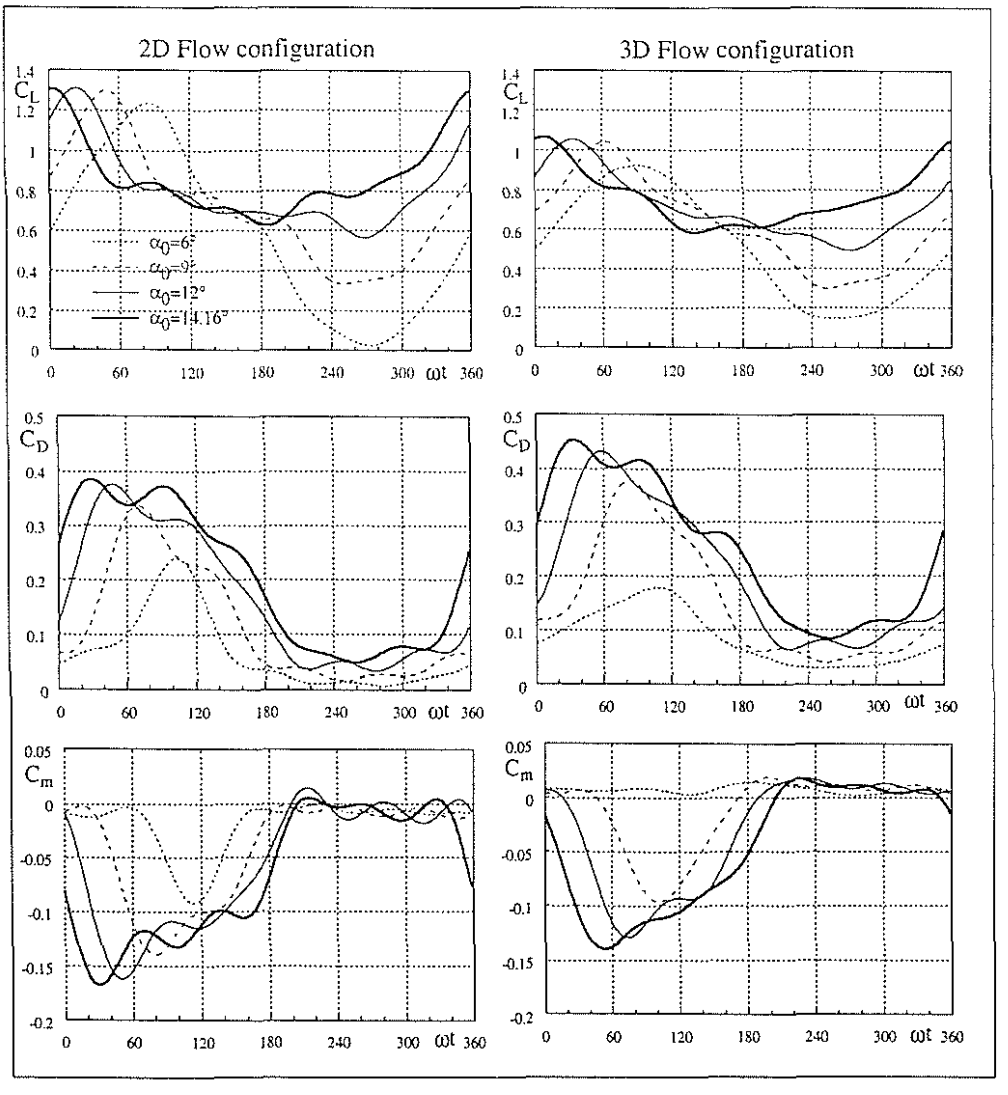

Figure 7 : Instantaneous Cl, Cd, Cm for case 1.

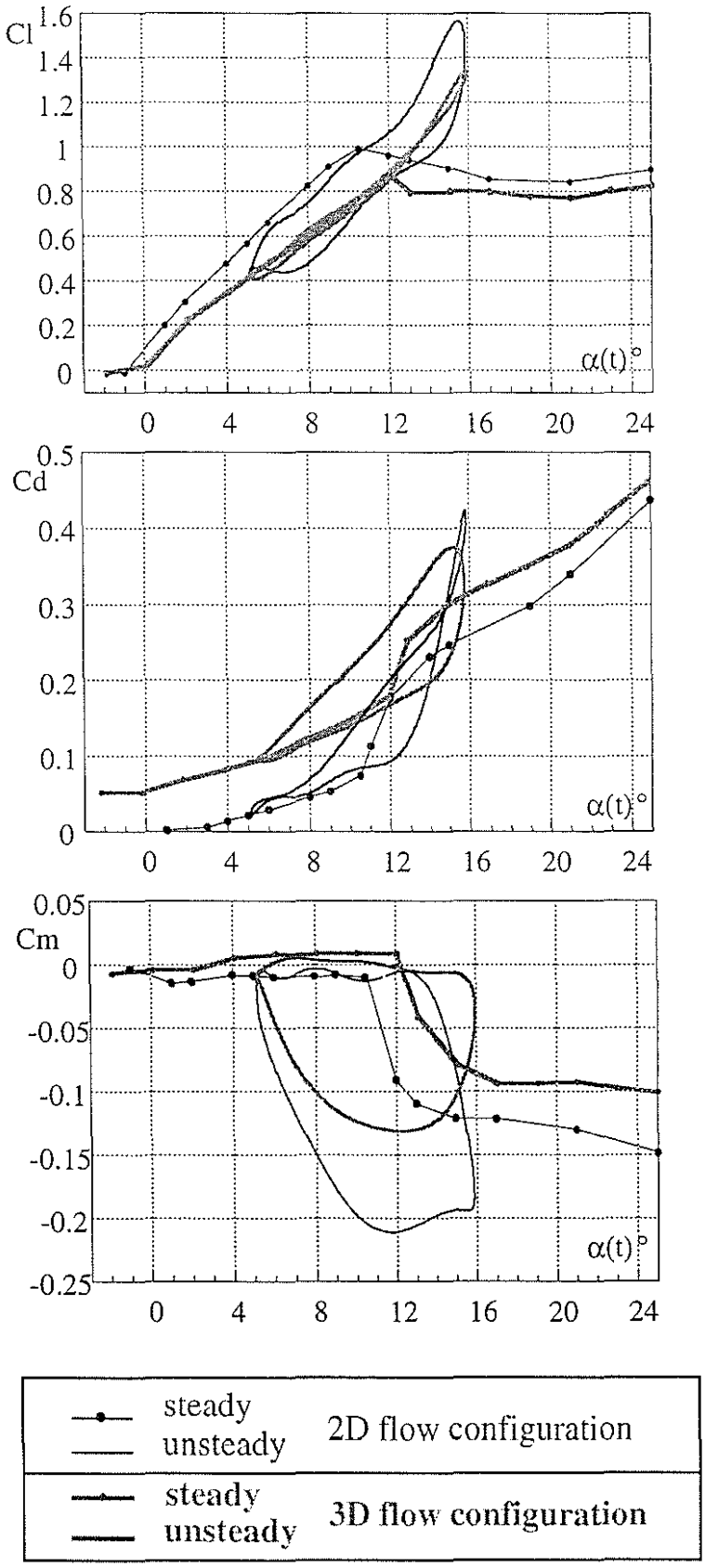

Figure 8 : Cl, Cd, Cm as a function of α(t) for case 5 - Combined Translation/Pitch motion, 2D and 3D flow configurations.

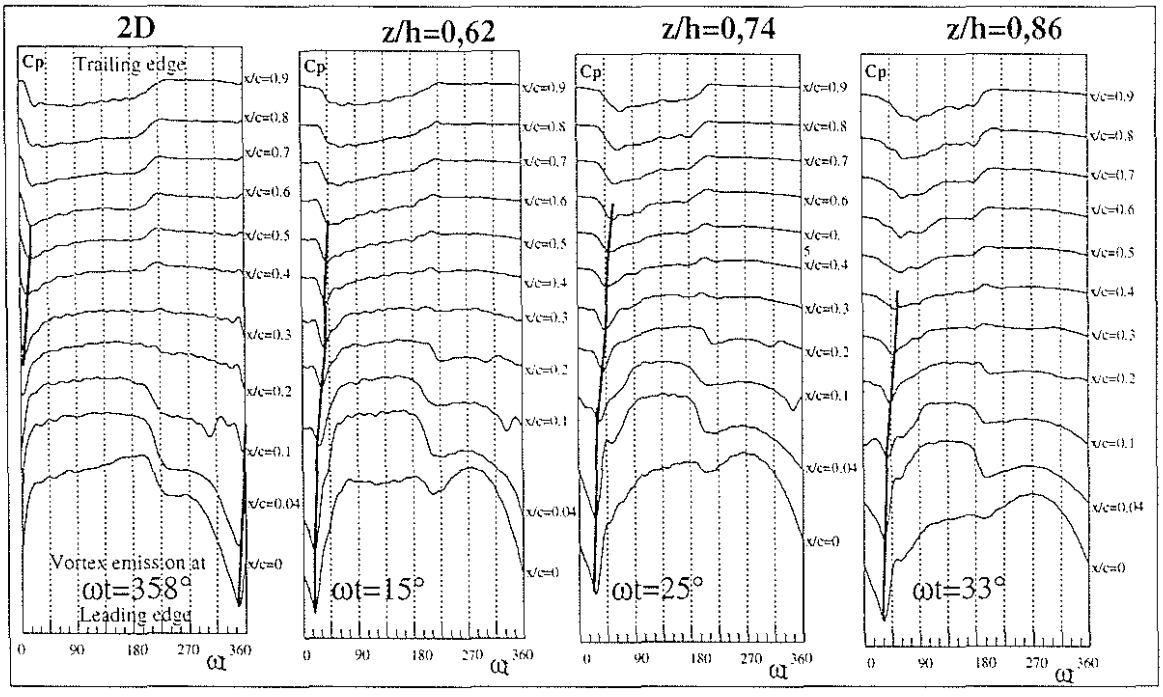

Figure 9 : Instantaneous Cp-distributions and stalling vortex propagation for case 1.

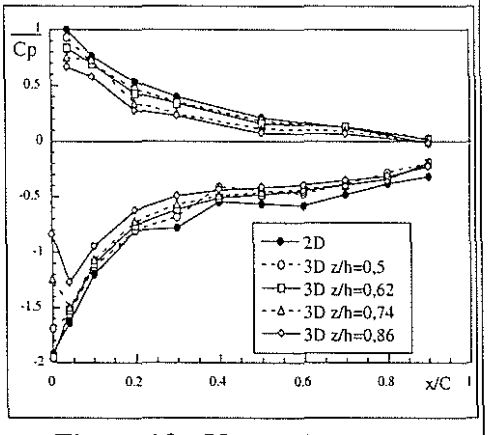

Figure 10 : Unsteady mean Cp-distribution for case 1.

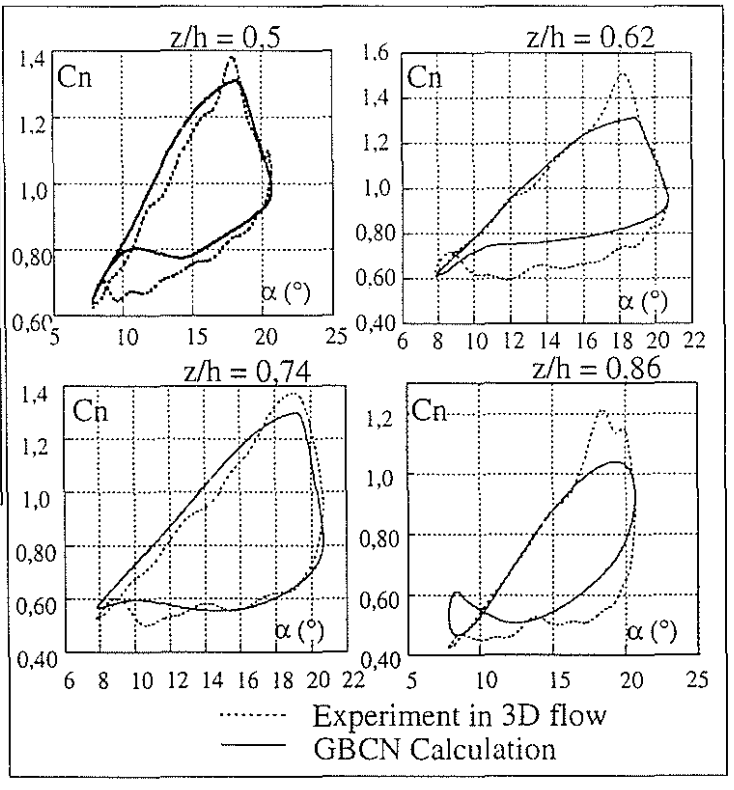

Figure 11 : Comparisons GBCN/experiment for case1.

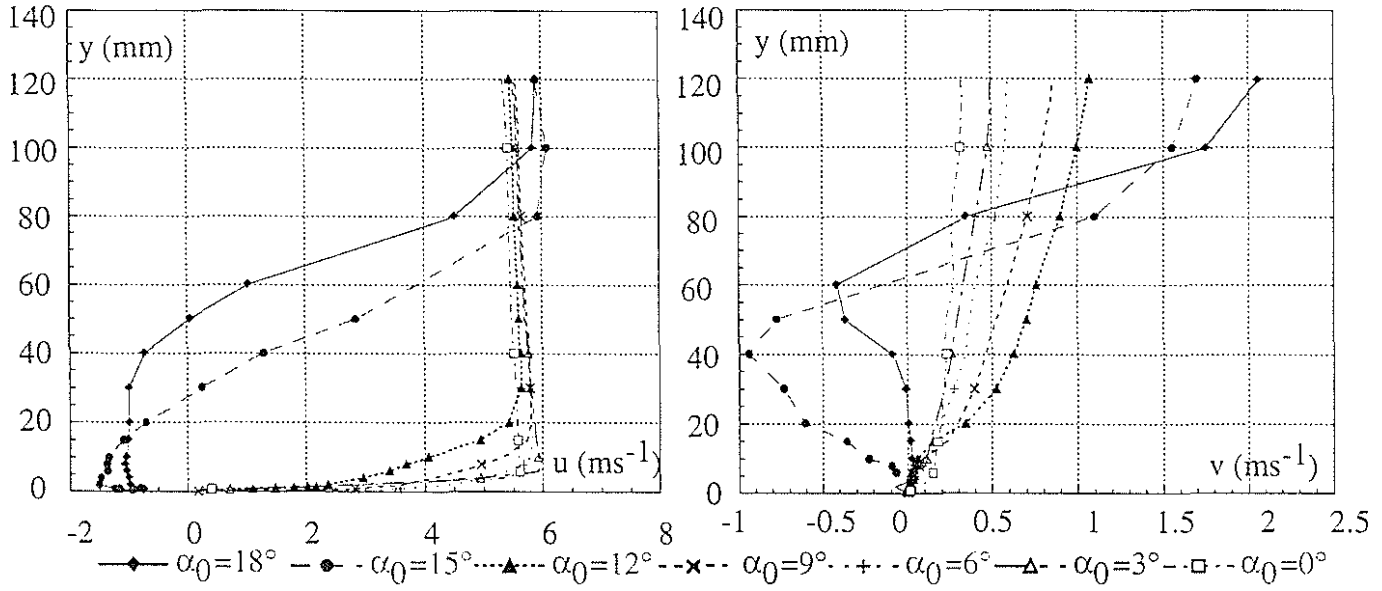

Figure 12 : Tangential and normal velocities (u,v) in steady flow as a function of α_0, $Re = 10^5$, s/c = 0.67

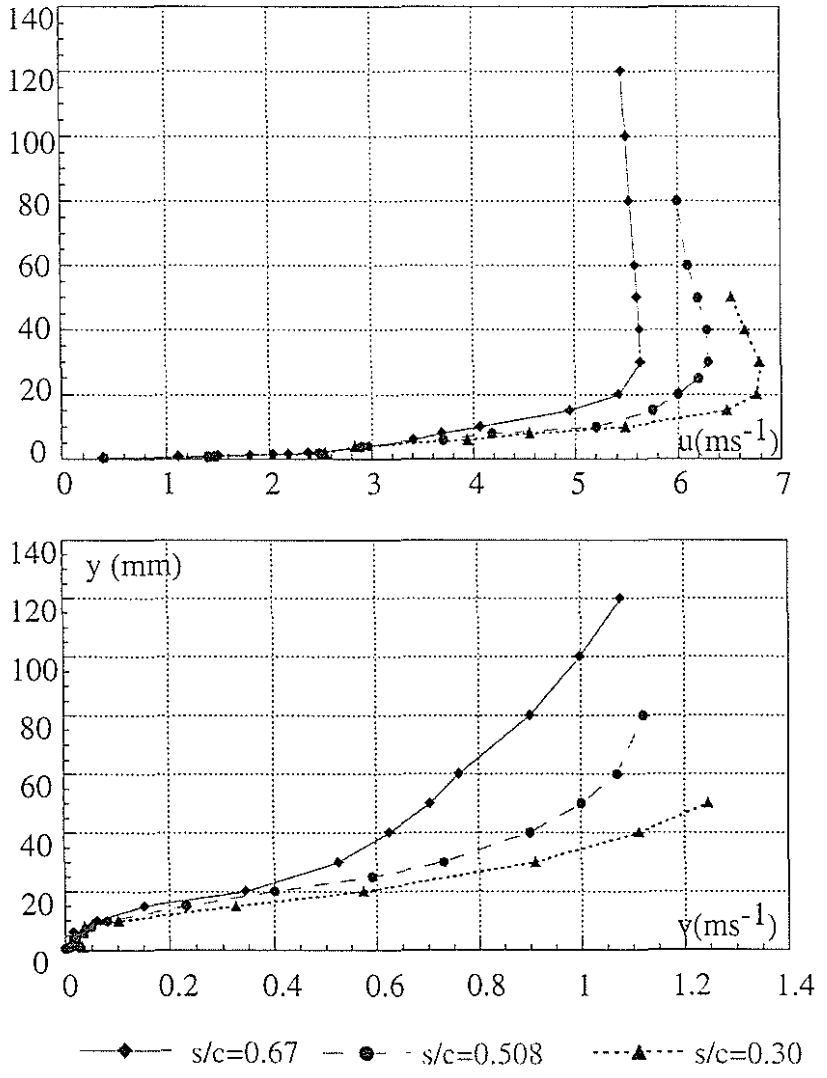

Figure 13 : Tangential and normal velocity profiles (u,v) in steady flow as a function of s/c, $Re = 10^5$, $\alpha_0 = 12°$

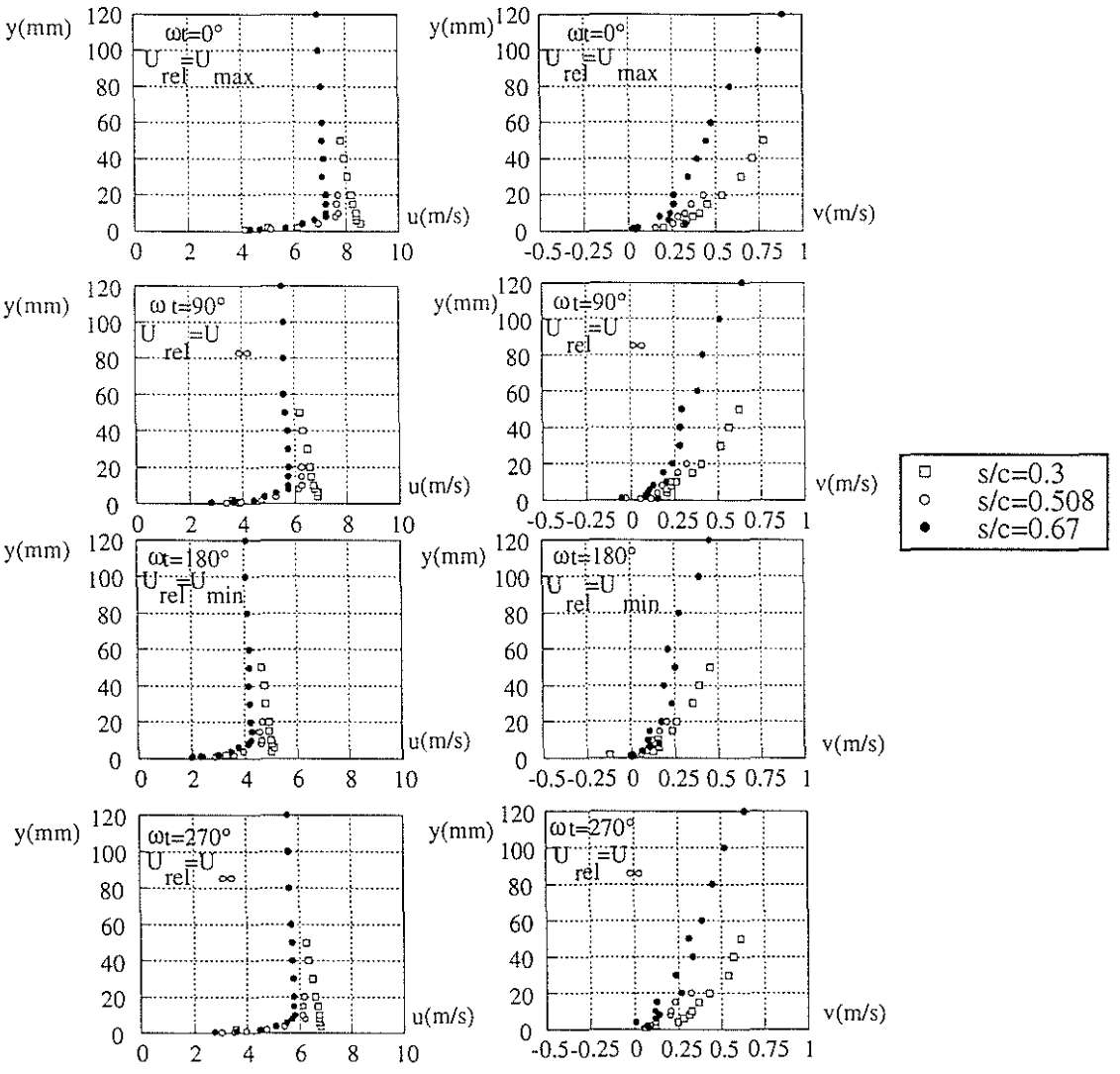

Figure 14 : Tangential and normal velocities (u,v) in fore-and-aft motion as a function of y and ωt, Re = 10^5, α_0 = 6°, λ = 0.251, k = 0.188

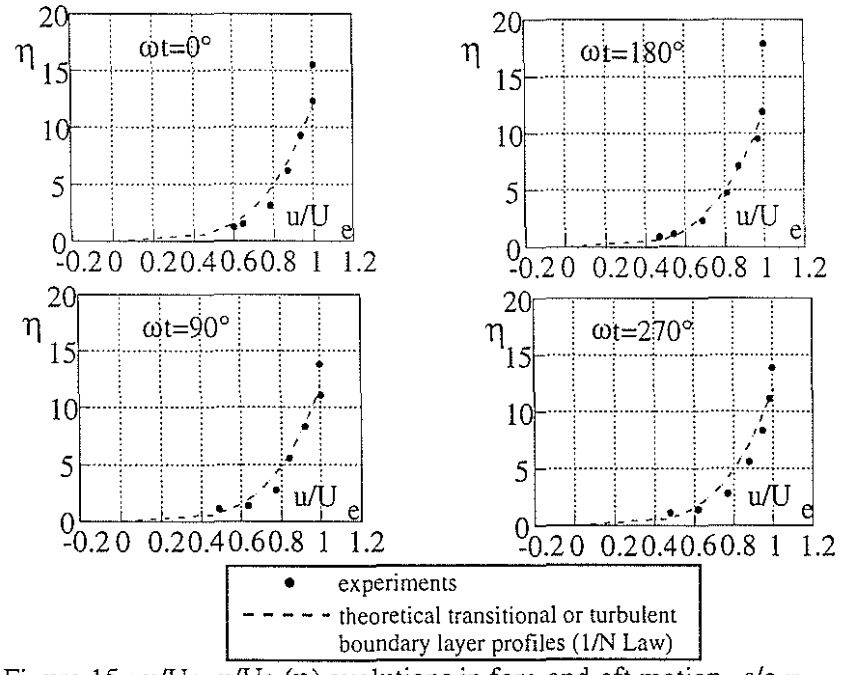

Figure 15 : u/Ue=u/Ue (η) evolutions in fore-and-aft motion , s/c = 0.67, Re = 10^5, α_0 = 6°, λ = 0.251, k = 0.188

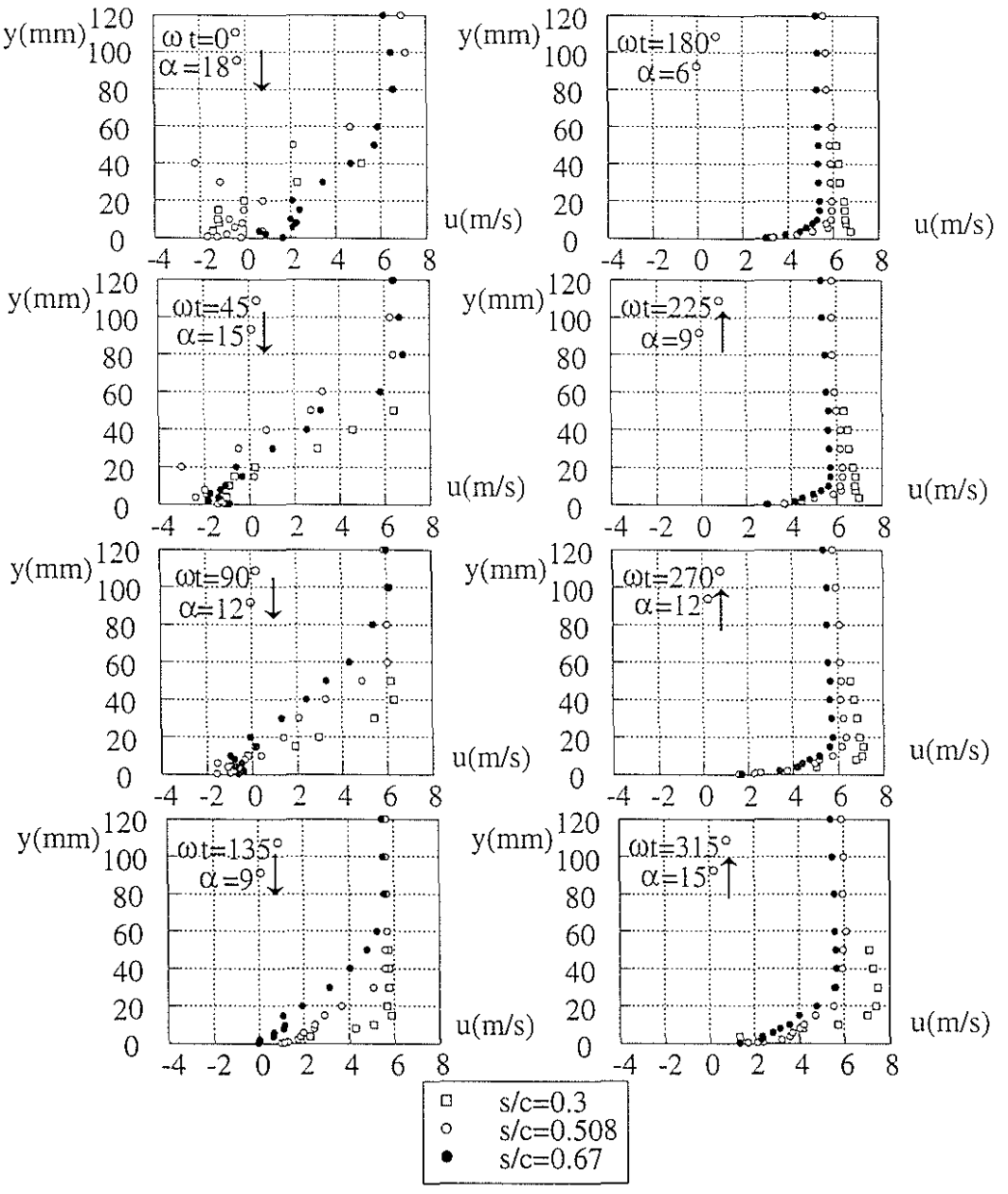

Figure 16 : Tangential velocitiy u=u(y,ωt) in pitching motion, Re = 10^5, $\alpha_0 = 12°$, $\Delta\alpha = 6°$, k = 0.188

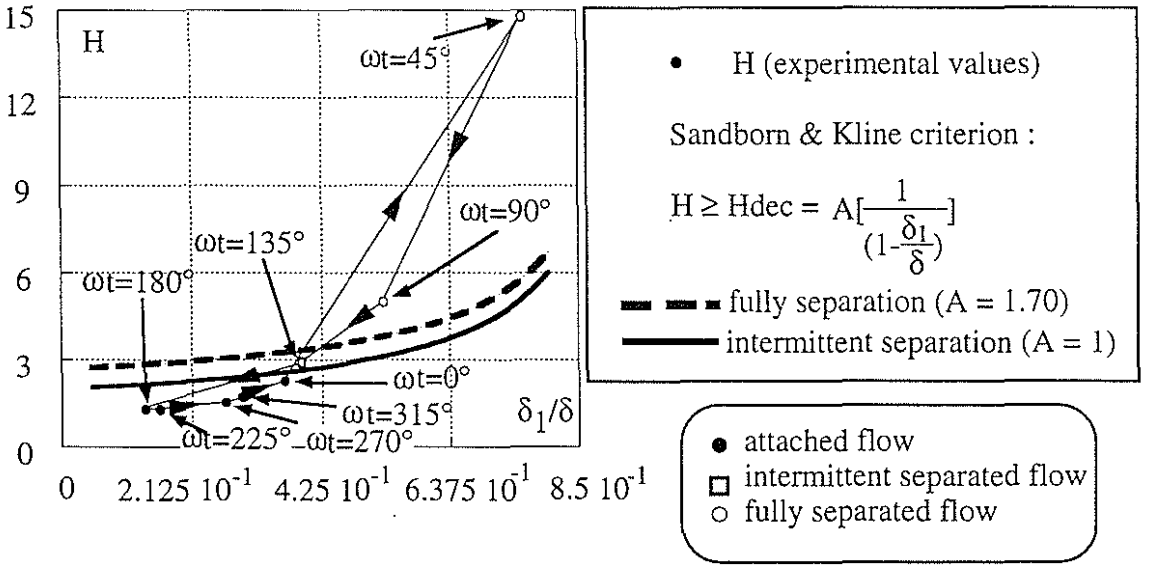

Figure 17 : Sandborn & Kline separation criterion in pitching motion, s/c = 0.67, Re = 10^5, $\alpha_0 = 12°$, $\Delta\alpha = 6°$, k = 0.188

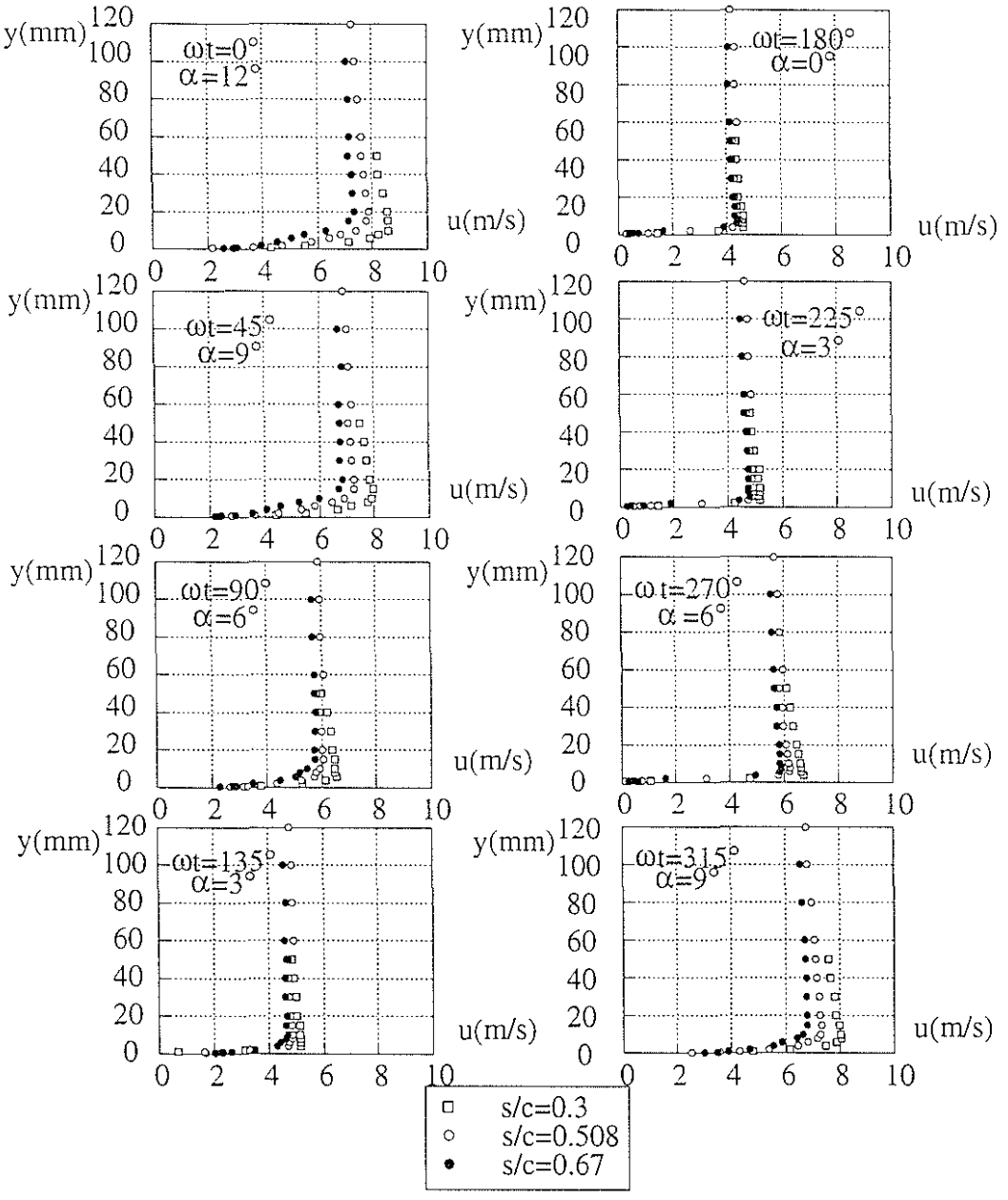

Figure 18 : Tangential velocitiy u=u(y,ωt) in translation/pitch combined motion, Re = 10^5, α_0 = 6°, $\Delta\alpha$ = 6°, λ = 0.251, k = 0.188, ϕ = 0°

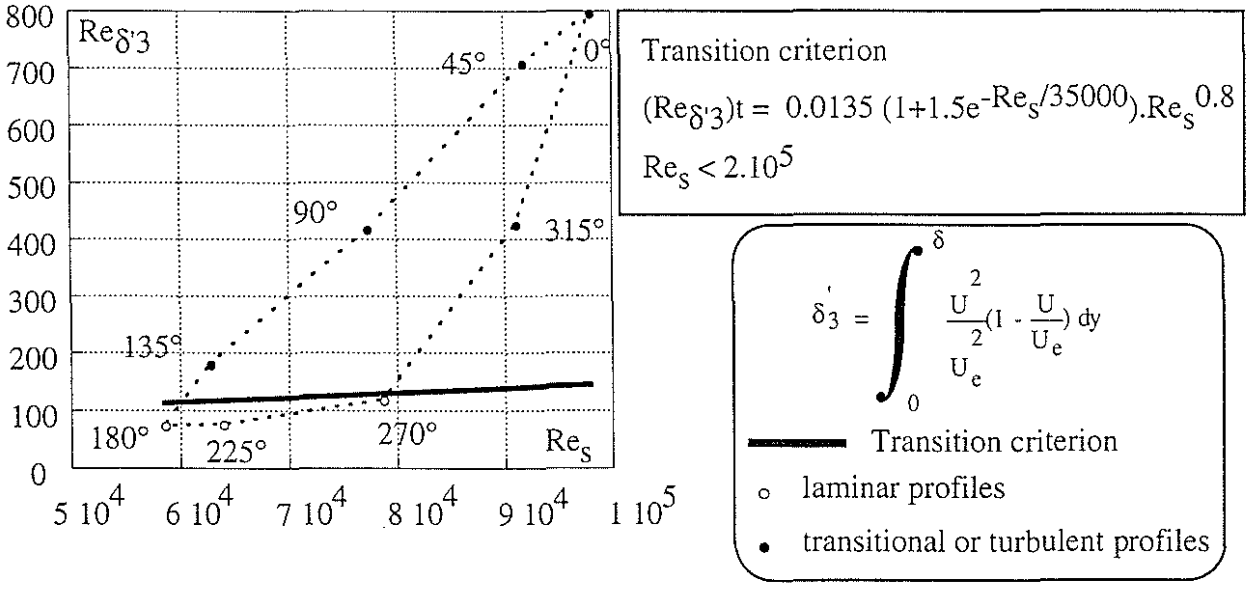

Figure 19 : Transition criterion in translation/pitch combined motion, s/c = 0.67, Re = 10^5, α_0 = 6°, $\Delta\alpha$ = 6°, λ = 0.251, k = 0.188, ϕ = 0°